International Journal of Signal Processing, Image Processing and Pattern Recognition
Vol.9, No.5, (2016), pp.357-372
http://dx.doi.org/10.14257/ijsip.2016.9.5.32

Simultaneous Intensity Inhomogensity Correction, Registration and Segmentation of Anatomical Structures From Brain MR Images

Yunjie Chen[1], Qin Xu[1], Yuhui Zheng[2], Jin Wang[3] and Jeong-Uk Kim[4]

[1] *School of Math and Statistic, Nanjing University of Information Science and Technology, Nanjing, China*
[2] *School of Computer and Software, Nanjing University of Information Science and Technology, Nanjing China*
[3] *School of Information Engineering, Yangzhou University, Yangzhou, China*
[4] *Department of Energy Grid, Sangmyung University, Seoul, Korea*

Abstract

Accurate segmentation for magnetic resonance (MR) images is an essential step in quantitative brain image analysis, and hence has attracted extensive research attention. However, due to the existence of noise and intensity inhomogeneity, also named as bias field, many segmentation methods suffer from limited accuracy. This paper presents a novel variational framework for the registration, segmentation and bias estimation simultaneously. We first presented an improved segmentation model by using the intensity statistic distributions with different means and variances in local regions. The model can estimate the bias field meanwhile segmenting images. We also proposed an anisotropic non-rigid registration method by using the structure tensor information and nonlocal information to contain the information of the image details. Finally, we defined a coupled term to combine the segmentation and registration. The registration term can provide shape information as a prior to guide the segmentation and the segmentation term can provide the edge information to guide the registration. The segmentation and registration can obtain benefit from each other. Our statistical results on both synthetic and clinical images show that the proposed method can overcome the difficulties caused by noise and bias fields and obtain more accurate results.

Keywords*: Bias field, Segmentation, Registration, Coupled framework*

1. Introduction

In order to diagnose brain disease, many segmentation methods have been proposed. Unfortunately, most segmentation methods are hindered by various imaging artifacts such as noise and intensity inhomogeneities. In order to obtain accurate anatomical structures from brain MR images, active contour models have been extensively applied [1-2]. The active contour models are several desirable than classical image segmentation methods, such as edge detection, thresholding, and region grow. The active contour models can be easily formulated into an energy minimization framework, which enable the models allow incorporate various prior knowledge, such as shape and intensity distribution, for robust image segmentation [3]. Furthermore, the active contour models can provide the segmentation results as smooth and closed contours, which can be readily used for further applications, such as shape analysis and recognition.

The active contour models can be categorized into two major classes: edge-based models and region-based models. Edge based models use edge information to attract the active contour toward the object boundaries, which makes the models sensitive to the noise [4]. Region based models identify the region of interest by using a certain region

ISSN: 2005-4254 IJSIP

descriptor to guide the motion of the active contour. Region based models are less sensitive to the noise [1], however, most of them tend to rely on intensity homogeneity in each of the regions to be segmented. In fact, due to technical limitations or artifacts introduced by the object being imaged, the medical images usually have intensity inhomogeneities. With the effect of the intensity inhomogeneity, the intensity varies within the same tissues. The variety usually less affects the human visual system; however, it may make the intensity distributions flatter in each tissue region. Segmentation experiments presented by Jungke *et al.*[5] illustrate that the intensity inhomogeneities affect the brain MR image segmentation more than the noise.

After the first paper has been proposed to estimate the bias field [6] in 1986, many methods have been proposed [7]. In the first decade, the methods relay on the information of the acquired images. The bias field estimation often by used as a preprocessing step, however, the estimation usually loses the detail information and makes the following segmentation inaccurate. In order to deal with this shortcoming, many segmentation and bias field estimation coupled methods have been proposed [8]. In the coupled methods, the bias field estimation and the segmentation can obtain benefit from each other.

In order to obtain more accurate results, Wang *et al.* proposed improved level set based method [4] by using the mean and variance information in a neighborhood around each pixel. However, these methods cannot obtain satisfied results when the bias field of the images is severe. Furthermore, although these methods can reduce the effect of the noise and bias field, they still cannot obtain accurate results in regions with severe low contrast.

In medical images, most structures contain priori shape information. Based on this assumption, a tremendous amount of registration based segmentation methods have been presented, see surveys [9]. The registration based segmentation methods need an atlas, which once has been constructed can be used as a template and can be registered to the image being segmented, to achieve the segmentation. The registration based segmentation methods usually have two processes. Firstly, they estimate the deformation field between the registered image and segmented image. Secondly, the estimated deformation field is applied to the atlas to achieve the segmentation.

The registration based segmentation methods can be categorized into two major classes: feature based and direct methods. The feature based methods require computation of enough features of points/surface/contours in the image and hence they need additional computational time in detecting the features. On the other hand, medical images usually have not enough distinctive features details, which makes the methods need interactive selection by an expert or by introducing extrinsic features, rigidly positioned with respect to the patient.

The direct methods estimate the transformation between the registered image and segmented image from the raw data. Wells and viola [10] proposed a novel direct method by using mutual information as a similarity measure. The scheme has been used in rigid and non-rigid registration. The mutual information based methods can be used without any preprocessing, user initialization or parameter tuning. However, when the overlapping part of the images is too small, the mutual information based methods are hard to find satisfied results. Furthermore, there are many local maxima in mutual information measure function, which cause problems with optimizer.

Among direct methods, a kind of approaches are based on the optical flow theory, which was firstly proposed by Horn and Schunck [11]. These methods use a global smoothness term to compute the optical flow. The optical flow method was first proposed for object tracking in image sequence. Because the displacement field and the velocity field in the optical flow model are similar to the registration. The optical flow method is based on the basis of the Taylor expansions and differential theory, and thus, it is weak to estimate large-scale movements between images. Furthermore, the optical flow method is sensitive to noises because it is on the basis of differential technology. In order to overcome this problem, some filters are used to reduce this bad effect, however, they may

lose edge information. Optical flow based methods usually assume that in the local neighborhood of every pixel is uniform; however, due to the effect of bias field, this assumption cannot be hold.

In order to obtain more accurate results, scholars attempt to joint registration and segmentation. Yezzi *et.al.*[12] and Paragios *et.al.* [13], proposed simultaneous registration and segmentation methods based on variational principle. These methods can improve the accuracy of the segmentation; however, they are based on rigid registration, which makes them hard to be used for brain MR image segmentation.

In this paper, we propose a coupled framework, which can process the registration, segment tissues and estimate the bias field, simultaneously. The registration can provide shape information as a prior to guide the segmentation and the segmentation results can make the registration more accurate. In order to reduce the effect of noise, we use statistical information (mean and variance) of local region around each pixel to construct the segmentation term and use the structure tensor information and nonlocal information to construct the registration term. The registration term can provide shape information as a prior to guide the segmentation and the segmentation term can provide the edge information to guide the registration. Another unique advantage of our method find accurate edges of the tissues with severe low contrast.

2. Methods

2.1. Simultaneous Intensity Inhomogeneity and Segmentation Method

The observed MRI image J can be regarded as the production of the true image I and the bias field B with the additive noise n [3]:

$$J = (I + n) \cdot B \tag{1}$$

In order to estimate the true image I, many methods take the logarithmic transform of both sides of Equation 1:

$$\log(J) = \log((I + n) \cdot B) = \log(I + n) + \log(B) \tag{2}$$

In this paper, we set $\log(J)$ as $\tilde{J}$, $\log(I + n)$ as $\tilde{I}$ and $\log(B)$ as $\tilde{B}$, respectively. Then, Equation 2 can be written as $\tilde{J} = \tilde{I} + \tilde{B}$.

In our previous work [3], we assumed that the bias field $\tilde{B}$ varies slowly over the entire image domain and the image intensity $\tilde{I}$ is fairly constant within each class of tissue in brain MR images. Let Ω be the image domain, $\{\Omega_i\}_{i=1}^{N}$ be a set of disjoint regions of the image. Then, $\Omega = \mathrm{U}\{\Omega_i\}_{i=1}^{N}, \Omega_i \mathrm{I}\ \Omega_j = \varnothing, \forall i \neq j$, where N is the number of regions. Due to the effect of the bias field, we model the intensities in the neighborhood Λ_Y of each pixel Y by Gaussian distribution. Based on our previous work in [3], the Gaussian probability density with varying means $\mu_i(Y)$ and variances $\sigma_i(Y)$ is defined as:

$$p_{i,Y}\left(\tilde{I}(X)\right) = \frac{1}{\sqrt{2\pi}\sigma_{i,Y}} \exp\left(-\frac{\left(\tilde{I}(X) - \mu_i(Y)\right)^2}{2\sigma_{i,Y}^2}\right), X \in \Lambda_Y \tag{3}$$

Where $\tilde{I}(X)$ is the intensity of X in the neighborhood Λ_Y of the current pixel Y. Furthermore, we uses the Gaussian kernel ω_σ with scale σ to reduce the effect of the noise and control the size of the neighborhood. Based on Maximum a posteriori probability(MAP), we can obtain the local energy function:

$$\varepsilon_Y = \sum_{i=1}^{N} \int_{\Omega_i} -\omega(X-Y) \log p_{i,Y}\left(\tilde{I}(X)\right) dX \tag{4}$$

Then, the ultimate goal is to minimize ε_Y for all the pixels Y in the image, which directs us to define the energy function as:

$$\varepsilon_{local} = \int_{\Omega} \sum_{i=1}^{N} \int_{\Omega_i} -\omega(X-Y) \log p_{i,Y}\left(\tilde{I}(X) - \tilde{B}(Y)\right) dX dY \tag{5}$$

The energy minimization can thus be performed by solving a level set evolution equation:

$$\varepsilon_{local} = -\int_{\Omega} \sum_{i=1}^{N} \left[\int_{\Omega_i} \omega(X-Y) \log p_{i,Y}\left(\tilde{I}(X) - \tilde{B}(Y)\right) M_i\left(\psi_1(X), \psi_2(X)\right) dX \right] dY \tag{6}$$

Where $M_i(\phi_1, \phi_2)$ are functions of ϕ ,such that $\sum_{i=1}^{N} M_i(\phi_1, \phi_2) = 1$. $H = \frac{1}{2}\left[1 + \frac{2}{\pi}\arctan\left(\frac{x}{\varepsilon}\right)\right]$ is the Heaviside function. In this paper, we set $N = 4$ and the image domain can be segmented into 4 regions corresponding to the white matter (WM), gray matter (GM), cerebrospinal fluid (CSF) and the background. $M_1(\phi) = H(\phi_1)H(\phi_2)$, $M_2(\phi) = H(\phi_1)(1 - H(\phi_2))$, $M_3(\phi) = (1 - H(\phi_1))H(\phi_2)$, $M_4(\phi) = (1 - H(\phi_1))(1 - H(\phi_2))$. The derivative of H is the smoothed Dirac delta function $\delta(x) = \frac{1}{\pi}\frac{\varepsilon}{\varepsilon^2 + x^2}$. For simplicity of notation, we denote $\phi = \{\phi_1, \phi_2\}$, $\Theta = \{u_1, u_2, u_3, u_4, \sigma_1, \sigma_2, \sigma_3, \sigma_4\}$ .The entire energy function can be written as:

$$\begin{aligned}
&E_{seg}\left(\tilde{B}, \phi, \Theta\right) \\
&= -\lambda_1 \int_{\Omega} \int_{\Omega_1} \omega(X-Y) \log p_{i,Y}\left(\tilde{I}(X) - \tilde{B}(Y)\right) M_1\left(\phi(X)\right) dX dY \\
&-\lambda_2 \int_{\Omega} \int_{\Omega_2} \omega(X-Y) \log p_{i,Y}\left(\tilde{I}(X) - \tilde{B}(Y)\right) M_2\left(\phi(X)\right) dX dY \\
&-\lambda_3 \int_{\Omega} \int_{\Omega_3} \omega(X-Y) \log p_{i,Y}\left(\tilde{I}(X) - \tilde{B}(Y)\right) M_3\left(\phi(X)\right) dX dY \\
&-\lambda_4 \int_{\Omega} \int_{\Omega_4} \omega(X-Y) \log p_{i,Y}\left(\tilde{I}(X) - \tilde{B}(Y)\right) M_4\left(\phi(X)\right) dX dY \\
&+\nu \int \left|\nabla H(\phi_1)\right| dY + \nu \int \left|\nabla H(\phi_2)\right| dY \\
&+\zeta \int \frac{1}{2}\left(\left|\nabla \phi_1\right| - 1\right)^2 dY + \zeta \int \frac{1}{2}\left(\left|\nabla \phi_2\right| - 1\right)^2 dY
\end{aligned} \tag{7}$$

where $\lambda_i, i=1,2,3,4$, ν and μ are nonnegative constant. $\int|\nabla H(\phi)|dY$ is the length of the zero level contour of ϕ to maintain a smooth contour, $\int\frac{1}{2}\left(|\nabla\phi|-1\right)^2 dY$ is the penalize term to regularize the level set.

2.2. Optical Flow Theory Based Registration Method

A general problem definition for optical flow theory based image registration can be posed as follows: Given two images $I(x,y,t)$ and $I(x,y,t+1)$, the optical flow is based on the assumption that grey values of images in subsequent frames do not change over time:

$$I(x+u,y+v,t+1)=I(x,y,t) \tag{8}$$

where the displacement field $(u,v)^T$ is called optical flow. Perform a first order Taylor expansion, the optical flow constraint

$$I_x u+I_y v+I_t=0 \tag{9}$$

The flow (u,v) cannot be computed locally without additional constraints [14]. So Horn *et.al.* added a smoothness constraint regularization term:

$$|\nabla u|^2+|\nabla v|^2 \tag{10}$$

where $|\nabla u|^2=\frac{\partial^2 u}{\partial x^2}+\frac{\partial^2 u}{\partial y^2}, |\nabla v|^2=\frac{\partial^2 v}{\partial x^2}+\frac{\partial^2 v}{\partial y^2}$ The basic idea underlying variational approaches is to recover the optical flow as a minimizer of the flow energy function:

$$E_{opt}(u,v)=\int_\Omega\left(I_x u+I_y v+I_t\right)^2 dxdy+\lambda\int_\Omega\left(|\nabla u|^2+|\nabla v|^2\right)dxdy \tag{11}$$

where the smoothness weight $\lambda>0$ serves as regularization parameter: Larger values for $\lambda>0$ result in a stronger penalisation of large flow gradients and lead to smoother flow fields. Minimising Equation 11 comes down to solving the Euler-Lagrange equations:

$$\left(I_x^2 u+I_x I_y v+I_x I_t\right)-\lambda\Delta u=0 \tag{12}$$

$$\left(I_y^2 v+I_x I_y u+I_y I_t\right)-\lambda\Delta v=0 \tag{13}$$

Where Δ is the spatial Laplace operator. The smoothness constraint regularization term can fill in information at location with $|\nabla I|\approx 0$. This results in dense flow fields and makes subsequent interpolation steps obsolete.

As we know, the spatial Laplace operator is isotropic, which makes the method inaccurate in edge region, furthermore, it is more sensitive to noise. In order to deal with this problem, we use nonlocal information to construct an anisotropic smoothness constraint regularization term.

Let us consider the noisy image $I:\Omega\to R^2$ defined on Ω. Barbu [15] has proposed PDE-based method to smooth images along defined directions of each pixels. In order to

smooth the image only along the directions of the edges, most of the denoising methods retrieve the local geometry of the image by using the diffusion tensor $D_X = \nabla I_X \nabla I_X^T$.

The eigenvectors μ^+ and μ^- of the tensor D_X can define the maximum and minimum variations of image intensities at X and the eigenvalues λ^+ and λ^- measure the variations along μ^+ and μ^-. We can find that the rank of D_X one and the eigenvalue of the tangent direction is zero. In order to retrieve a more coherent geometry, a Gaussian-smoothed version $D_\sigma = G_\sigma * D$ is usually computed.

In order to smooth the images on the desired directions, Weickert *et al.* [16] defined a new diffusion tensor D' as:

$$D_X' = f^+_{\left(\lambda^+,\lambda^-\right)}\mu^+\mu^{+T} + f^-_{\left(\lambda^+,\lambda^-\right)}\mu^-\mu^{-T}, \forall X \in \Omega \tag{14}$$

where f^+ and f^- control the strength along the desired directions μ^+ and μ^-. Following the idea of the improved diffusion tensor, we have defined $f^-\left(\lambda^+,\lambda^-\right)=1$ and $f^+\left(\lambda^+,\lambda^-\right)=\exp\left(-C\times\left(\lambda^+-\lambda^-\right)\right)$ in our previous work [17]. With this definition, $f^+\left(\lambda^+,\lambda^-\right)$ is less than 1 in the edge regions and near to 1 in homogeneous regions. As analyzed in [43], in this paper, we set $C=1/90$.

The diffusion tensor is based on the gradient of each pixel's intensity, which makes it sensitive to the noise. We use the Nonlocal information to improve the diffusion tensor. The traditional NonLocal framework has been widely used for image denoising. The basic idea of the nonlocal framework is using the local patch information of each pixels of the image to update the intensity of the current pixel:

$$R(x) = \frac{\int_\Omega I(y)\omega(x,y)dy}{\int_\Omega \omega(x,y)dy}, \forall x \in \Omega \tag{15}$$

With

$$\omega(x,y) = e^{-\|P_x - P_y\|^2/h^2} \tag{16}$$

The weight function $\omega(x,y)$ measures the similarity between patches centered at x and y with width $2\times p+1$. The points, whose neighborhood are more similar, will have a larger weight and are more probably, belong to the same tissue. h is a nonnegative number to control the decay of the exponential function[46]. In practical implementations, the denoising methods only search pixels in a small window with radius r for computational purposes. Then the eigenvectors μ^+ and μ^- of the tensor D can be improved as:

$$\mu_X^+ = \frac{\int_\Omega \mu_Y^+\omega(X,Y)dY}{\int_\Omega \omega(X,Y)dY} \tag{17}$$

$$\mu_X^- = \frac{\int_\Omega \mu_Y^-\omega(X,Y)dY}{\int_\Omega \omega(X,Y)dY} \tag{18}$$

Then Equation 12 and Equation 13 can be improved as:

$$\left(I_x^2 u + I_x I_y v + I_x I_t\right) - \lambda div\left(D'\nabla v\right) = 0 \tag{19}$$

$$\left(I_y^2 v + I_x I_y u + I_y I_t\right) - \lambda div\left(D'\nabla v\right) = 0 \tag{20}$$

3. Simultaneous Intensity Inhomogeneity Correction, Registration and Segmentation Method

Let I_1 be the reference image containing the atlas table T_1, I_2 be the float image that needs to be segmented, $(u,v)^T$ be the vector field. The segmentation and registration coupled framework is given as :

$$\min E\left(\phi,u,v,\%,\Theta\right) = E_{seg}\left(I_2,\%,\phi,\Theta\right) + E_{\mathrm{Re}g}\left(I_1,I_2,u,v\right) + E_{Cou}\left(u,v,\phi,T_1\right) \tag{21}$$

where, the first term denotes the segmentation functional, the second term denotes the registration functional and the third term measures the distance between the transformed atlas $T_1(x+u,y+v)$ and the current segmentation ϕ .Then, the simultaneous intensity inhomogeneity correction, registration and segmentation model can be written as:

$$\begin{aligned}
&E\left(\phi,u,v,\%,\Theta\right)\\
&= -\lambda_1\int_\Omega\int_{\Omega_1}\omega(X-Y)\log p_{i,Y}\left(\%(X)-\%(Y)\right)M_1\left(\phi(X)\right)dXdY\\
&-\lambda_2\int_\Omega\int_{\Omega_2}\omega(X-Y)\log p_{i,Y}\left(\%(X)-\%(Y)\right)M_2\left(\phi(X)\right)dXdY\\
&-\lambda_3\int_\Omega\int_{\Omega_3}\omega(X-Y)\log p_{i,Y}\left(\%(X)-\%(Y)\right)M_3\left(\phi(X)\right)dXdY\\
&-\lambda_4\int_\Omega\int_{\Omega_4}\omega(X-Y)\log p_{i,Y}\left(\%(X)-\%(Y)\right)M_4\left(\phi(X)\right)dXdY\\
&+\nu\int\left|\nabla H\left(\phi_1\right)\right|dY + \nu\int\left|\nabla H\left(\phi_2\right)\right|dY\\
&+\zeta\int\frac{1}{2}\left(\left|\nabla\phi_1\right|-1\right)^2 dY + \zeta\int\frac{1}{2}\left(\left|\nabla\phi_2\right|-1\right)^2 dY\\
&+\int_\Omega\left(I_x u + I_y v + I_t\right)^2 dxdy + \lambda_5\int_\Omega\left(\nabla u^T D\nabla u + \nabla v^T D\nabla v\right)dxdy\\
&+\lambda_6\int_\Omega\frac{1}{2}\left(T_1(x+u,y+v) - H\left(\phi(x,y)\right)\right)^2 dxdy
\end{aligned} \tag{22}$$

3.1. Numerical Technique

For fixed u , v , $\%$, Θ , the minimization of $E\left(\phi,u,v,\%,\Theta\right)$ can be solved by using the gradient descent method:

$$\frac{\partial \phi_1}{\partial t} = -\delta(\phi_1)(-\lambda_1 e_1 H(\phi_2) - \lambda_2 e_2 (1 - H(\phi_2)) + \lambda_3 e_3 H(\phi_2) + \lambda_4 e_4 (1 - H(\phi_2)) + \nu\delta(\phi_1) div\left(\frac{\nabla \phi_1}{|\phi_1|}\right) + \zeta\left(\nabla^2 \phi_1 - div\left(\frac{\nabla \phi_1}{|\phi_1|}\right)\right) + \lambda_6 \delta(\phi_1)\left(T_1^{\#} - H(\phi_1)\right) \quad (23)$$

Where, $T_1^{\#}(x, y) = T_1(x + u, y + v)$ and

$$e_i(y) = \int \omega(x - y)\left[\log(\sigma_i(x)) + \frac{(J(x) - B(y) - u_i(x))^2}{2\sigma_i(x)^2}\right] dx \quad (24)$$

In the same manner, we can obtain the gradient descent flow of ϕ_2:

$$\frac{\partial \phi_2}{\partial t} = -\delta(\phi_2)(-\lambda_1 e_1 H(\phi_1) + \lambda_2 e_2 H(\phi_1) - \lambda_3 e_3 (1 - H(\phi_1)) + \lambda_4 e_4 (1 - H(\phi_1)) + \nu\delta(\phi_2) div\left(\frac{\nabla \phi_2}{|\phi_2|}\right) + \zeta\left(\nabla^2 \phi_2 - div\left(\frac{\nabla \phi_2}{|\phi_2|}\right)\right) + \lambda_6 \delta(\phi_2)\left(T_1^{\#} - H(\phi_2)\right) \quad (25)$$

For fixed ϕ, B, u, v, we find an optimal μ and σ that minimizes E. By some calculus manipulations, μ and σ can be given as

$$\mu_i(X) = \frac{\int \omega * (J(Y) - B(X)) M_i(\phi) dY}{\int \omega * M_i(\phi) dY} \quad (26)$$

$$\sigma_{i,X}^2 = \frac{\int \omega * (J(Y) - B(X) - u_i(X))^2 M_i(\phi) dY}{\int \omega * M_i(\phi) dY} \quad (27)$$

For fixed ϕ, μ, σ, u and v, B can be obtained by minimum E:

$$B(X) = \frac{\sum_{i=1}^{N} \lambda_i \int \omega(X - Y) \frac{|J(Y) - u_i(x)|}{\sigma_i^2} M_i(\phi) dY}{\sum_{i=1}^{N} \lambda_i \int \omega(X - Y) \frac{1}{\sigma_i^2(X)} M_i(\phi) dY} \quad (28)$$

For fixed ϕ, μ, σ and B, the minimization of Equation (23) comes down to solving its corresponding Euler-Lagrange equations. They are given by:

$$\left(I_x^2 u + I_x I_y v + I_x I_t\right) - \lambda_3 div(D\nabla u) + \lambda_5 \left(T_1 + T_{1,x} u + T_{1,y} v - H(\phi(x, y)) T_{1,x}\right) = 0 \quad (29)$$

$$\left(I_x I_y u + I_y^2 v + I_y I_t\right) - \lambda_3 div(D\nabla v) + \lambda_5 \left(T_1 + T_{1,x} u + T_{1,y} v - H(\phi(x, y)) T_{1,y}\right) = 0 \quad (30)$$

Our model for simultaneous intensity inhomogeneity correction, segmenting and registration can be summarized as follows:

Step 1. Initialize ϕ, Θ, B, u and v.

Step 2. Update ϕ by using Equation (23) and (25).

Step 3. Update μ_i, σ_i by using Equation (26) and Equation (27).

Step 4. Update B by using Equation (28).

Step 5. Update u, v by using Equation (29) Equation (30).

Step 6. Repeat Steps (2-5) until the stop requirement is achieved.

4. Implementation and Results

In this section, we tested the proposed method on both synthetic and real images acquired using different modalities. For all experiments shown in this paper, we set the parameters $\sigma = 5$ for ω in Equation (4), $\lambda_i = 1, i = 1,2,3,4,5$, $\zeta = 1$, $\nu = 0.001 \times 255^2$ and $\lambda_6 = 200$.

The first experiments are carried out on 3T-weighted brain MR images. Three MR slices, together with the estimated bias fields, bias corrected images, and segmentation results are shown in Figure 1. The first column shows the reference images and the 2nd column shows the segmentation results of the reference images. It shows that the intensities within each brain tissue in the bias corrected images become quite homogeneous. Figure 1 demonstrates that the results of our method are consistent with the expected tissue regions.

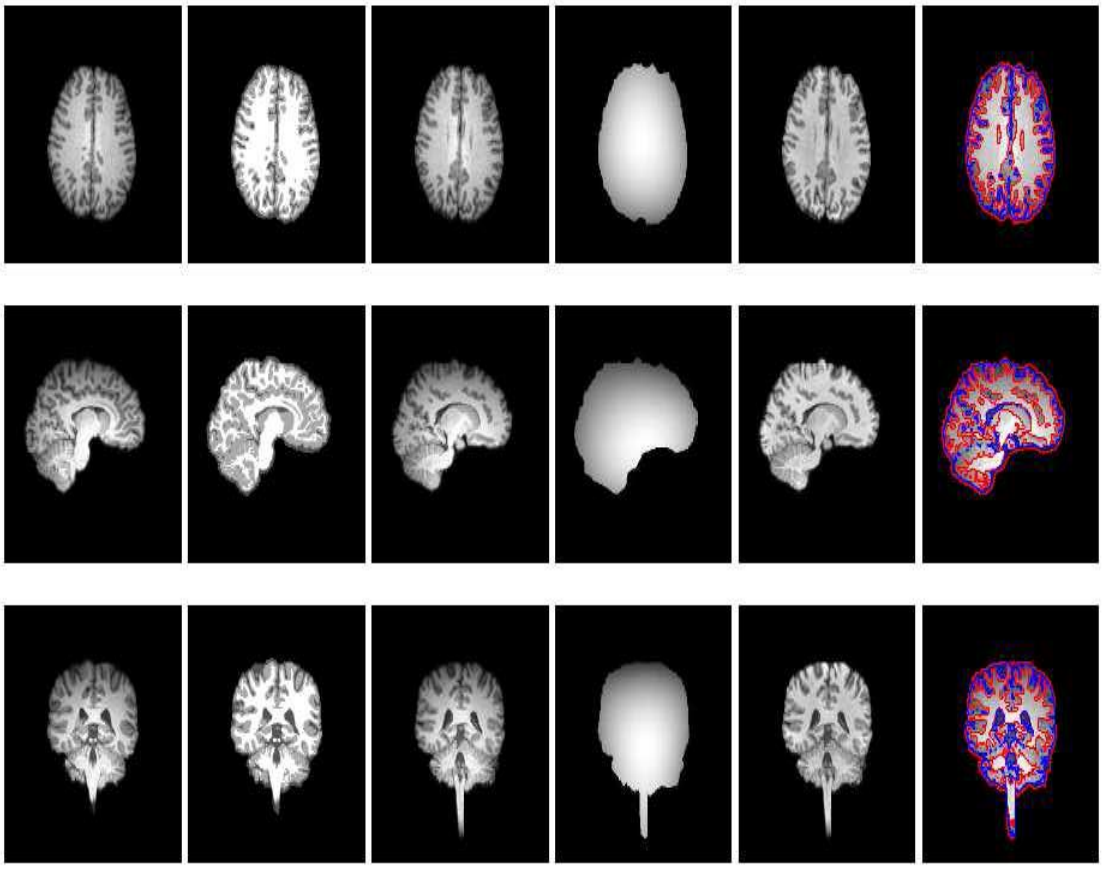

Figure 1. Illustration of Three 3T-Weighted Brain MR Images, (1st Column) Reference Image, (2nd Column) Atlas of the Reference Image, (3rd Column)the Images to be Segmented, (4th Column) Their Estimated Bias Fields, (5th Column) Bias-Corrected Images, and(6th Column) Segmentation Results of the Proposed Algorithm

In the second experiment, we quantitatively compared our method with four existing segmentation methods, including Li's method [47], Ji's method [15], Nonlocal information based Fuzzy Clustering method (NLFCM) [45] and LGD method[8]. The parameters for each method are set with the default values specified in the papers. All five methods are tested on the synthetic images, which were created with the MRI simulator (Brain Web, Brain Imaging Center at the Montreal Neurological Institute, McGill University). The simulator can provide full three-dimensional data volumes which have been simulated using three sequences(T1-,T2-,and PD- weighted) and a variety of slice thicknesses, noise levels and intensity inhomogeneity levels; provides the ground truth of the image data. In this manuscript, the parameters of the simulated data sets are: Phantom: normal, Slice thickness:1mm, Scan technique: SFLASH, TR=18 msec, flip angle =30 degrees, TE=10 msec. The dimension of the image data sets is 181×217×181. In order to show the robustness of the methods on the noise, we applied all these methods on the 87th transaxial image with the noise levels: noise levels 1%, 3%, 4% and 5%. All these images have the same intensity inhomogeneity level 30%. The results are shown in Figure 2.

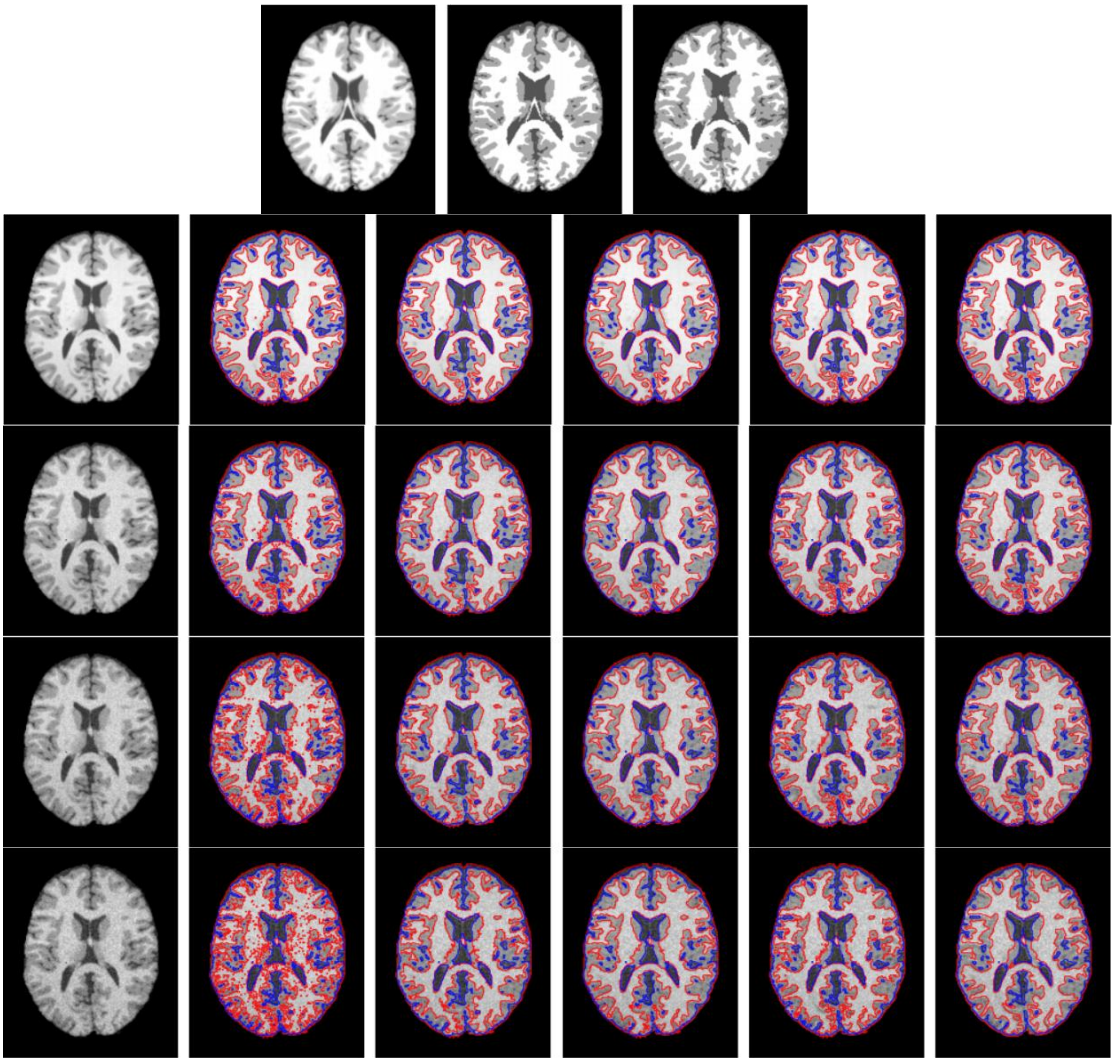

Figure 2. Illustration of Simulated Four Transaxial Images (87th from BrainWeb). The First Row Shows the Reference Image, the Ground Truth of the Reference Image and the Ground Truth of the 87th Image, Respectively. The 1st Column Show the Initial Images with Parameters: Noise Levels 1%, 3%, 4%and 5%, Respectively and Same Intensity Inhomogeneity Level 30%.

From the 2nd Column to the Right Column Show the Results of Li's Method, Ji's Method, NLFCM, LGD Method and Our Method, Respectively

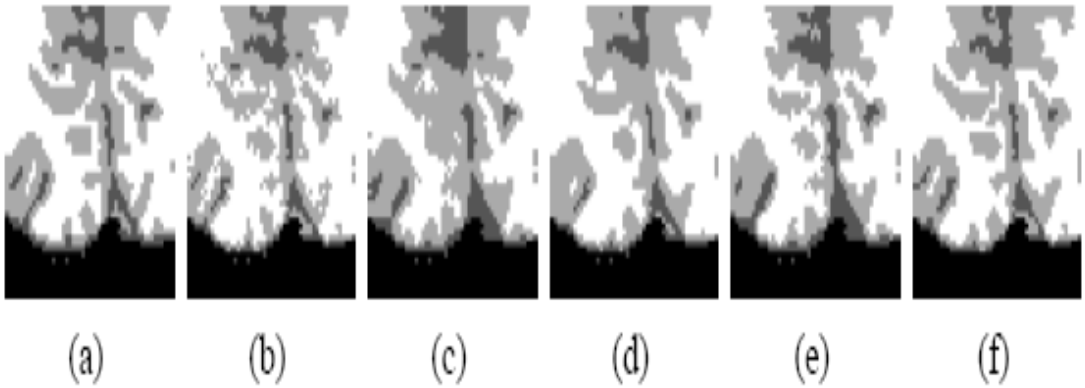

Figure 3. Details of the Results on the 87th Transaxial Image of a Simulated Image with Parameters: Noise Levels 3% and Intensity Inhomogeneity Level 30%. (a) The Ground Truth. (b) The Result of Li's Method, (c) The Result of Ji's Method, (d) The Result of NLFCM, (e) The Result of LGD Method, (f) The Result of Our Method

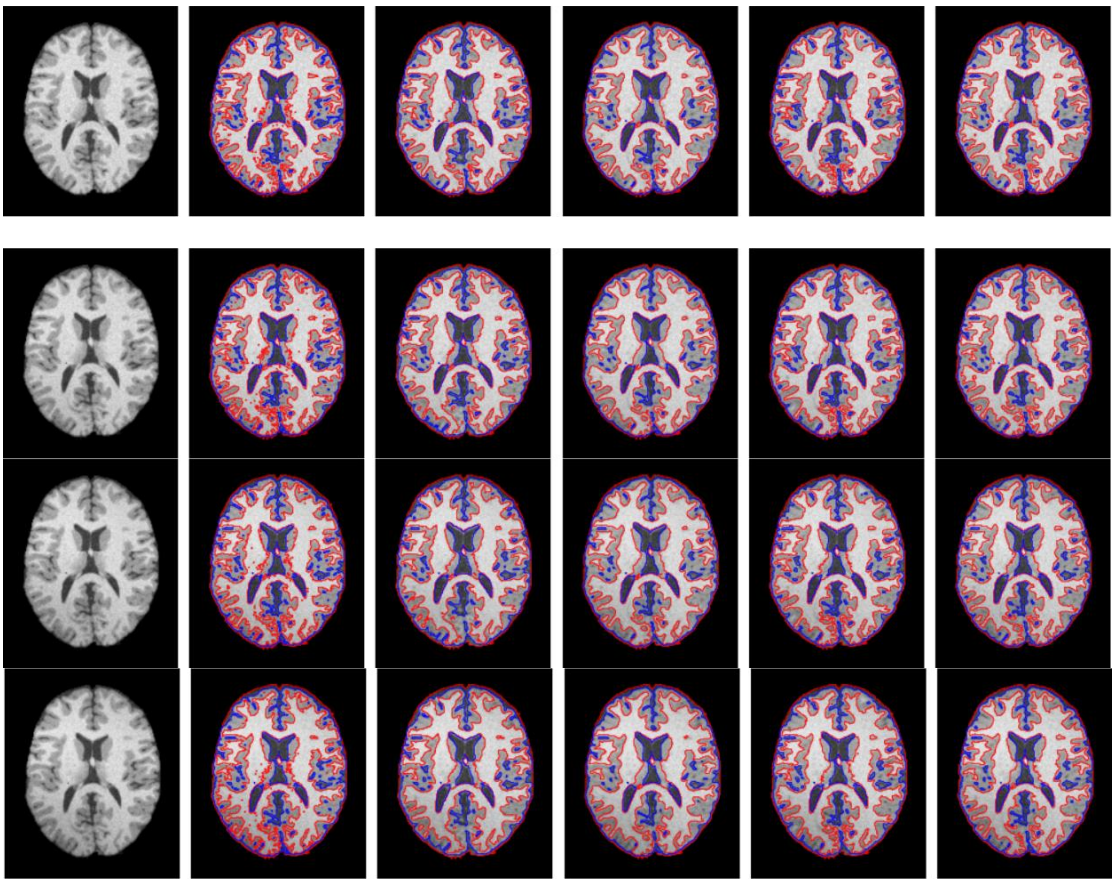

Figure 4. Illustration of Simulated Four Transaxial Images (87th from BrainWeb). The 1st Column Show the Initial Images with Parameters: Intensity Inhomogeneity Levels 20%, 40%, 60% and 80%, Respectively and the Same Noise Level 3%. From the 2nd Column to the Right Column Show the Results of Li's Method, Ji's Method, NLFCM, LGD Method and Our Method, Respectively

The first column shows the initial images and the second column shows the segmentation results of Li's method. The Li's method can reduce the effect of the bias field; however, it is based on the k-method and only uses the intensity information of each pixels, which makes it sensitive to the noise. From the results, we can find that the Li's method cannot obtain satisfied results when the noise level increases. The third column shows the segmentation results of the Ji's method. In order to reduce the effect of the noise, the method proposed spatial information amongst neighborhood pixels based on the posterior probabilities, prior probabilities and the spatial direction information. We can find that the Ji's method can reduce the effect of the noise. However, Ji's method is based on FCM, which makes it hard to segment tissues with low contrast. Figure 3 shows the details of the results on the 87th transaxial image of a simulated image with parameters: noise levels 3% and intensity inhomogeneity level 30%. The details of the Ji's method are shown in Figure3.(c) and from the result we can find that the method is hard to distinguish the transition region between the tissues. The NLFCM reduce the effect of the noise by using nonlocal patch information of each pixel and the results can be seen in the 4th column of Figure 2. The NLFCM only uses the isotropic patch information, which makes it cannot obtain the results of tissues with slim structures. The details of the segmentation results can be seen in Figure 3.(d) and from the result, we can find that some CSF have been misclassified into GM. The LGD method models the intensities of each tissues by a spatial Gaussian distribution in local regions of each pixel, which can segment images meanwhile estimate the intensity inhomogeneities. The right column of Figure 2 shows the results of our method. From the results we can find that the LGD method cannot obtain satisfied results in some transition regions. The results of our method can be seen in the right column of Figure 2. In our method, we use the information of local region intensity distribution to construct the segmentation energy, use nonlocal information to guide the registration, and coupled the segmentation and registration to obtain the best results.

In order to show the robustness to the bias field, we compared our method with Li's method [19], Ji's method [8], Nonlocal information based Fuzzy Clustering method (NLFCM)[18] and LGD method [3] on the 87 the transaxial image with the parameters: intensity inhomogeneity levels 20%, 40%, 60% and 80%, respectively and the same noise levels 3%.

The first column of the Figure 4 shows the initial image. In this experiment, we use the same reference image as shown in Figure 2. The second column shows the segmentation results of the Li's method. The Li's method estimates the bias field by using basis function. However, this method is sensitive to the noise and when the inaccurate results may make the method trapped into local optima. The segmentation results of the Ji's method are shown in the 3rd column. From the result, we can find that the method can reduce the effect of the noise by using local neighbor information of each pixel. As illustrated before, Ji's method find accurate results in area with low contrast. The fourth column shows the segment results of the NLFCM method. The NLFCM method reduce the effect of the bias field by defining a regular term, which needs uses the intensity information of the local neighborhood of each pixel. This method has high computational cost and cannot estimate the bias field. This method cannot obtain satisfied results in the areas with low contrast. The fifth column shows the segmentation results of the LGD method. The method can segment images meanwhile estimate the intensity inhomogeneities. However, the bias field is depend on the accuracy of the segmentation, more accurate segmentation results can make the method obtain more accurate estimated bias field. The method cannot obtain accurate results in the area with low contrast. The segmentation results of our method are shown in the right column and are more robust than other methods.

To facilitate the visions, we compare the proposed algorithm with the other relative methods on simulated brain MR images. The performance of segmentation was evaluated

quantitatively by using the Jaccard similarity (JS), which is the ratio between intersection and union of the segmented volume S_1 and ground truth volume S_2.

$$JS(S_1, S_2) = \|S_1 \cap S_2\| / \|S_1 \cup S_2\| \tag{31}$$

The value of JS ranges from 0 to 1, with a higher value presenting a more accurate segmentation result. To statistically show the significant of the proposed method, we apply above five methods to the segmentation of 40 whole simulated MR image data sets, in which the level of noise ranges from 3% to 9%. The accuracy of the segmentation is measured by the average JS value, and the statistical results (means and standard deviations of JS values for WM, GM and CSF) are listed in Table 1. The results demonstrate that our method produces the most accurate results and has the best ability and robustness to the noisy images (with lower standard deviations of JS values and higher mean of JS values when the noise increases), especially in the area with abundant textures (with higher JS values for CSF tissue). We also apply above five methods to the segmentation of 40 whole simulated MR image data sets, in which the level of intensity inhomogeneity ranges from 20% to 100%. The segmentation accuracy is measured in terms of the average JS of WM, GM and CSF delineation, and is shown in Figure 5. Both visual and quantitative comparisons show that the our method is more robust to the intensity inhomogeneity and can obtain more accurate results.

Table 1. The Average JS Values (Mean ± Standard Deviation) of GM, WM and CSF Segmentation Obtained by Applying Five Algorithms to T1-Wighted Brain MR Images with Increasing Level of Noise.

Algorithm	Tissues	3%	5%	7%	9%
Li's method	WM GM CSF	0.9182±0.078 0.9062±0.048 0.8937±0.052	0.7831 ± 0.065 0.7914 ± 0.046 0.7624 ± 0.065	0.7100 ± 0.046 0.7250 ± 0.036 0.7023 ± 0.069	0.6814±0.038 0.6753±0.032 0.6649±0.042
Ji's method	WM GM CSF	0.9265±0.054 0.9156±0.023 0.9143±0.021	0.9069 ± 0.061 0.8387 ± 0.019 0.8911 ± 0.031	0.8825 ± 0.065 0.8216 ± 0.039 0.8711 ± 0.032	0.8631±0.066 0.8076±0.021 0.8421±0.041
NLFCM	WM GM CSF	0.9214±0.024 0.9286±0.041 0.9103±0.028	0.8735 ± 0.031 0.8626 ± 0.049 0.8541 ± 0.037	0.8625 ± 0.034 0.8716 ± 0.019 0.8427 ± 0.041	0.8432±0.041 0.8264±0.052 0.8268±0.046
LGD	WM GM CSF	0.9212±0.037 0.9236±0.026 0.9167±0.029	0.9037±0.041 0.9108±0.037 0.9061±0.035	0.8912±0.045 0.8979±0.049 0.8820±0.030	0.8811±0.037 0.8851±0.046 0.8713±0.029
our method	WM GM CSF	0.9401±0.019 0.9391±0.017 0.9303±0.022	0.9367±0.036 0.9307±0.032 0.9289±0.033	0.9286±0.037 0.9245±0.037 0.9207±0.029	0.9152±0.035 0.9128±0.033 0.9119±0.031

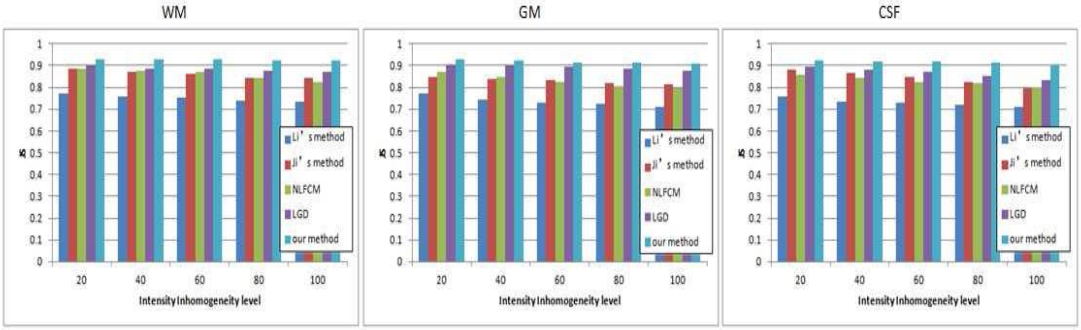

Figure 5. Average JS Values of the Segmentation Results of WM(Left), GM(Middle) and CSF(Right) Obtained by Applying Five Segmentation Methods to Simulated Brain MR Images with Increasing Levels of Intensity Inhomogeneity

4. Conclusion

In this paper, we proposed a simultaneous intensity inhomogeneity correction, registration and segmentation coupled method. The method can obtain more accurate results, especially for brain tissues with low contrast, by coupling the registration and integrating the bias field estimation model into the objective function. This method successfully overcomes the drawbacks of existing simplex segmentation schemes, including limited robustness to outliers, over-smoothness for segmentations, and limited segmentation accuracy for image details. Our results of both synthetic and real images show that the proposed model can largely overcome the difficulties raised by noise, intensity inhomogeneity, low contrast and is capable of producing more accurate segmentation results than several state-of-the-art algorithms.

Acknowledgements

This paper is a revised and expanded version of a paper entitled “An automatical segmentation method for brain MR images” presented at CST 2016 China, April 22-23. This work was supported in part by the National Nature Science Foundation of China 61572257, 61402234; National Research Foundation of Korea under Grant NRF-2013K2A2S2000777; Natural Science Foundation of Jiangsu Province BY2014007-04, BK20150923. It was also supported by the Industrial Strategic Technology Development Program (10041740) funded by the Ministry of Trade, Industry and Energy (MOTIE) Korea. Prof. Jeong-Uk Kim is the corresponding author.

References

[1] T. Chan and L. Vese, “Active contours without edges,” *IEEE Trans. Imag. Proc.*, vol. 10, no. 2, **(2001)**, pp. 266–277.
[2] Y. Chen, B. Zhao, J. Zhang and Y. Zheng, “Automatic segmentation for brain mr images via a convex optimized segmentation and bias field correction coupled model,” Magnetic Resonance Imaging, vol. 32, no. 5, **(2014)**, pp. 941–955.
[3] Q. Song, J. Bai, M. Garvin, M. Sonka, J. Buatti and X.Wu, “Optimal multiple surface segmentation with shape and context priors,” IEEE Transcations on medical imageing, vol. 32, no. 2, **(2013)**, pp. 376 – 386.
[4] L.Wang, F. Shi,W. Lin, J. Gilmore and D. Shen, “Automatic segmentation of neonatal images using convex optimization and coupled level sets,” Neuroimage, vol. 58, no. 3, **(2011)**, pp. 805–17.
[5] M. Jungke, W. Seelen, G. Bielke, M. Grigat and P. Pfannenstiel, “A system for the diagnostic use of tissue characterizing parameters in nmr-tomography,” in Information Processing in Medical Imaging, **(1987)**, pp. 471–481.
[6] J. Haselgrove and M. Prammer, “An algorithm for compensating of surface-coil images for sensitivity of the surface coil,” Magn. Reson. Imag., vol. 4, **(1986)**, pp. 469–472.

[7] U. Vovk, F. Pernus and B. Likar, "A review of methods for correction of intensity inhomogeneity in mri," IEEE Transcations on medical imageing, vol. 26, no. 3, **(2007)**, pp. 405–421.
[8] Z. Ji, J. Liu, G. Cao, Q. Sun and Q. Chen, "Robust spatially constrained fuzzy cmeans algorithm for brain mr image segmentation," Pattern Recognition, vol. 47, no. 7, **(2014)**, pp. 2454–2466.
[9] P. Markelj, D. Tomazvic, B. Likar and F. Pernus, "A review of 3d/2d registration methods for image-guided interventions," Medical Image Analysis, vol. 16, no. 3, **(2012)**, pp. 642–661.
[10] W. Wells, P. Viola, H. Atsumi, S. Nakajima and R. Kikinis, "Multimodal volume registration by maximization of mutual information," Med. Image Anal., vol. 1, no. 1, **(1996)**, pp. 35–51.
[11] B. Horn and B. Schunck, "Determining optical flow," Artificial Intelligence, vol. 17, no. 1, , **(1981)**, pp. 185C203.
[12] L. Z. A. Yezzi and T. Kapur, "A variational framework for integrating segmentation and registration through active contours," Medical Image Analysis, vol. 7, no. 2, **(2003)**, pp. 171–185.
[13] N. Paragios, M. Rousson and V. Ramesh, "Knowledge-based registration & segmentation of the left ventricle," in WACV, **(2002)**, pp. 37–42.
[14] B. K. Horn and B. G. Schunck, "Determining optical flow," Artificial Intelligence, vol. 17, no. 1, **(1981)**, pp. 185–203.
[15] T. Barbu, "Robust anisotropic diffusion scheme for image noise removal," Procedia Computer Science, vol. 35, no. 8, **(2014)**, pp. 522–530.
[16] W. J, H. R. BM and V. MA, "Efficient and reliable schemes for nonlinear diffusion filtering," IEEE Trans on Image Process, vol. 7, no. 3, **(1998)**, pp. 398–410.
[17] Y. Chen, J. Zhang, and J. Yang, "An anisotropic images segmentation and bias correction method," Magnetic Resonance Imaging, vol. 30, no. 1, **(2012)**, pp. 85–95.
[18] B. Caldairou, N. Passat, P. Habas, C. Studholme and F. Rousseau, "Robust spatially constrained fuzzy c-means algorithm for brain mr image segmentation," Pattern Recognition, vol. 44, no. 9, **(2011)**, pp. 1916–27.
[19] C. Li, C. Gatenby, L.Wang and J. C. Gore, "A robust parametric method for bias field estimation and segmentation of mr images," in CVPR, **(2009)**, pp. 218 – 223.

Authors

Yunjie Chen, Dr Yunjie Chen received his PHD degree in 2008 from Nanjing University of Science & Technology. His main research interests include image processing, pattern recognition and numerical analysis.

Jin Wang Dr. Jin Wang received the B.S. and M.S. degree from Nanjing University of Posts and Telecommunications, China in 2002 and 2005, respectively. He received Ph.D. degree from Kyung Hee University Korea in 2010. Now, he is a professor in the School of Information Engineering, Yangzhou University. His research interests mainly include routing method and algorithm design, performance evaluation and optimization for wireless ad hoc and sensor networks. He is a member of the IEEE and ACM.

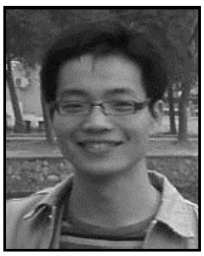

Yuhui Zheng Dr. Yuhui Zheng received his PHD degree in 2009 from Nanjing University of Science & Technology. His main research interests include image processing, pattern recognition and numerical analysis.

Jeong-Uk Kim received his B.S. degree in Control and Instrumentation Engineering from Seoul National University in 1987, M.S. and Ph.D. degrees in Electrical Engineering from Korea Advanced Institute of Science and Technology in 1989, and 1993, respectively. He is an associated professor at the SangMyung University in Seoul. His research interests include smart grid demand response, building automation system, and renewable energy.